

QUANTIFYING IMPACTS OF CLIMATE CHANGE AND VARIABILITY ON
GROUNDWATER RECHARGE IN TULELAKE, CALIFORNIA

A Thesis submitted to the faculty of
San Francisco State University
In partial fulfillment of
the requirements for
the Degree

Master of Science

In

Geoscience

by

Hannah Morgan Dailey

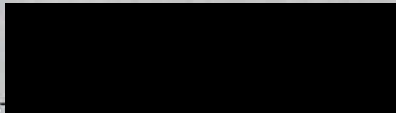
San Francisco, California

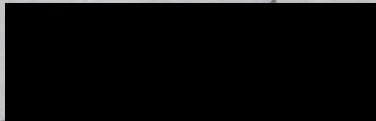
May 2020

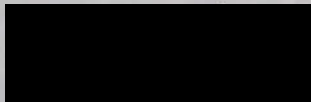
Copyright by
Hannah Morgan Dailey
2020

CERTIFICATION OF APPROVAL

I certify that I have read QUANTIFYING IMPACTS OF CLIMATE CHANGE AND VARIABILITY ON GROUNDWATER RECHARGE IN TULELAKE, CALIFORNIA by Hannah Morgan Dailey, and that in my opinion this work meets the criteria for approving a thesis submitted in partial fulfillment of the requirement for the degree Master of Science in Geoscience at San Francisco State University.


Dr. Yadira Ibarra, Ph.D.
Assistant Professor


Dr. Jason Gurdak, Ph.D.
Associate Professor



Dr. Leora Nanus, Ph.D.
Assistant Professor

QUANTIFYING IMPACTS OF CLIMATE CHANGE AND VARIABILITY ON GROUNDWATER RECHARGE IN TULELAKE, CALIFORNIA

Hannah Morgan Dailey
San Francisco, California
May 2020

Understanding how climate change and variability will interact with groundwater resources is crucial for sustainable groundwater management. To better understand this relationship at the management scale, I investigate the effects of interannual to multidecadal climate variability on groundwater resources of the Tulelake Irrigation District (TID) in northern California using singular spectrum analysis (SSA) and lag correlations. The SSA results indicate that while the El Niño-Southern Oscillation (ENSO) and Pacific Decadal Oscillation (PDO) influence precipitation, streamflow, and groundwater levels, there is a larger contribution of PDO-like variability in the groundwater levels but with low to moderate lag correlation coefficients. I also explored the effects of future climate change by using HYDRUS-1D models to simulate recharge beneath the two dominant soil textures (Tulebasin clay and Laki sandy loam) of the TID from 1950 to 2099 using downscaled output from four global climate models (GCMs) at representative concentration pathways (RCP) 4.5 and 8.5. Median recharge values range from 77 to 182 mm/year for the Tulebasin and Laki sediments, with the greatest recharge rates simulated during the historic time period (1950 to 2005). Although simulated recharge rates under the RCP 4.5 and 8.5 scenarios are not statistically different, they are statistically significant and as much as 50% lower simulated recharge during the end of the 21st century as compared to the historic time period. The simulated decreasing trend in future recharge is more sensitive to decreases in air temperature and evapotranspiration than increases in average annual precipitation. Moreover, the semi-arid climate and relatively shallow depth to water (<4 m) of the TID create recharge dynamics that are relatively sensitive to forecasted air temperature and evapotranspiration. The findings from this thesis can be used by water resources managers in the TID or other similar agencies to forecast future groundwater budgets and plan for the likely decreases in recharge over the coming decades of the 21st century.

I certify that the Abstract is a correct representation of the content of this thesis.



Chair, Thesis Committee



Date

ACKNOWLEDGEMENTS

There are many people to thank for their continual encouragement and support while working on this project. Dr. Jason Gurdak has played an integral role in my journey at San Francisco State and with his guidance and encouragement has led me to achieve many academic and professional opportunities. Additionally, I would like to thank my committee members Dr. Yadira Ibarra and Dr. Leora Nanus for their continual kind words of encouragement and insightful comments and questions.

I would like to thank the numerous friends and family who have traveled with me on this long journey. I am grateful to my partner and family whose unwavering confidence and support has encouraged me even in the most challenging of times. Additionally, I would like to thank the many friends who have supported me in my time at San Francisco State including my fellow cohort – Natasha Fazeli, Drew Lowdermilk, and Kara Cowan – as well as Cassandra Wolf – whose knowledge, kindness, and support has contributed to my success.

Finally, I would like to acknowledge Dr. Karen Grove and Jay Ach, David Dawdy, and Ray Pestrong for continuing to fund student research by providing research awards such as the Professor Emeritus Karen Grove and Jay Ach Fellowship, the David Dawdy Hydrologic Research Award, and Ray Pestrong Research Award to students in the Earth and Climate Sciences department. These donors have played a critical role in funding graduate research and this project would not be possible without their generous support.

TABLE OF CONTENTS

List of Figures	ix
List of Tables	x
1.0 Introduction.....	1
1.1 Climate Variability and Groundwater Resources	2
1.2 The El Niño-Southern Oscillation	3
1.3 The Pacific Decadal Oscillation.....	4
1.4 Study Area	5
1.5 Scope and Purpose	7
2.0 Methodology.....	8
2.1 Data Selection	8
2.1.1 Observed Data.....	9
2.1.2 Simulated Data.....	10
2.2 Time Series Analysis	11
2.2.1 Data Pre-Processing	11
2.2.2 Single Spectrum Analysis	12
2.2.3 Lag Correlation	15
2.3 Spatial Variation Analysis	16
2.4 Groundwater Recharge Analysis	17
2.4.1 Hydrus-1D.....	17
2.4.2 Model Calibration	20

3.0 Results and Discussion	21
3.1 Variation of Climate Variability in Hydrologic Time Series.....	21
3.2 Lag Correlation	23
3.2.1 Climate.....	23
3.3 Spatial Variation in Groundwater Levels in the TID.....	25
3.4 Groundwater Recharge in the TID.....	27
3.4.1 Spin Up Results by Soil Texture.....	27
3.4.2 Groundwater Recharge in the TID by Time Period.....	28
4.0 Conclusion	31
5.0 References.....	34
6.0 Figures.....	38
7.0 Tables	48

LIST OF FIGURES

Figures	Page
1. Timeseries of the MEI and PDO Indices.....	38
2. Location of the observed data stations and map of the Tulelake Irrigation District, Tulelake, California.....	39
3. Soil map of the Tulelake Irrigation District from the STATSGO2/SSURGO USDA NCRS database.....	40
4. Lag correlation plots of PDO and MEI indices to hydrologic time series	41
5. Box plots of depth to water measurements (e.g., groundwater levels) for three wells that are distributed in the northeast, northwest, and southeast quadrants in the Tulelake Irrigation District.....	42
6. Cumulative annual recharge from 1950-2099 for the Tulebasin and Laki sediments in the Tulelake Irrigation District.....	43
7. Cumulative annual recharge for the Tulebasin and Laki sediments by time period for the representative concentration pathway (RCPs) 4.5 and 8.5. Results from the Steel-Dwass test are shown above with letters denoting statistical differences from the historic time period.....	44
8. Cumulative annual precipitation by time period with historic and future projections from representative concentration pathways (RCPs) 4.5 and 8.5. Results from the Steel-Dwass test are shown above with letters denoting statistical differences from the historic time period, and asterisks denoting differences between 4.5 and corresponding 8.5 RCP datasets.....	45

9. Temperature by time period with historic and future projections from representative concentration pathways (RCPs) 4.5 and 8.5 of the global climate model (GCMs) datasets. Lower values correspond to minimum temperature, and higher values correspond to maximum temperature. Results from the Steel-Dwass test are shown with letters denoting statistical differences from the historic time period, and asterisks denoting differences between RCP 4.5 and corresponding 8.5 RCP datasets.....46

10. Evapotranspiration rate by time period for the cereal grains crop type with historic and future projections from representative concentration pathways (RCPs) 4.5 and 8.5 of the global climate model (GCMs) datasets. Results from the Steel-Dwass test are shown with letters denoting statistical differences from the historic time period.....47

LIST OF TABLES

Table	Page
1. Summary of time series data used in the SSA and lag correlation analysis.....	48
2. Soil properties for the Tulebasin and Laki sediments that are used as input for HYDRUS-1D models.....	48
3. The percent variance of the composite reconstructed components (RCs) attributed to the El Niño-Southern Oscillation (ENSO), Pacific Decadal Oscillation (PDO), and >PDO for the hydrologic time series.....	49
4. Results of the climate index to hydrologic time series lag correlations. Correlations are denoted between the Pacific Decadal Oscillation (PDO) and the El Niño-Southern Oscillation (ENSO) composite reconstructed components (RCs) of climate indices and hydrologic time series lag correlations.....	50

1.0 Introduction

Groundwater is an important freshwater resource and component of the hydrologic cycle. This water resource supports ecosystem functions, public and domestic water supplies, irrigation water for agriculture, and other industrial uses. During drought, groundwater is often used when surface water resources are not available in a management practice known as conjunctive use. However, in many parts of the world, especially arid and semi-arid regions, groundwater is mismanaged and the resulting impacts on water quality and water quantity threaten the sustainability of the local freshwater resources. Groundwater sustainability challenges are further exacerbated by climate variability and climate change (Green et al. 2011; Taylor et al., 2012); thus understanding the response in groundwater resources to such climate perturbations is important to help inform best management practices and policy decisions (Famiglietti 2014; Meixner et al. 2016).

In 2014, California passed the Sustainable Groundwater Management Act (SGMA), which signified a statewide shift in water resource management towards sustainability. Through basin prioritization, defining sustainable yield, and mitigation of undesirable results, SGMA aims to achieve sustainable groundwater use by 2040 for critically overdrafted groundwater basins and by 2042 for high and medium priority groundwater basins (CA DWR 2017). Given that groundwater supports many sectors of California's economy, understanding how the impacts of climate change and climate variability may influence groundwater resources is a critical aspect of sustainable management.

1.1 Climate Variability and Groundwater Resources

Climate variability and climate change can directly and indirectly influence many components of a groundwater budget, including recharge (Meixner et al. 2016). Climate variability can occur on all spatial and temporal scales, beyond singular weather or storm events. Specifically, climate variability is defined as the difference between the current climatic conditions and the mean climatic conditions, which are calculated over longer temporal scales (Kuss and Gurdak, 2014). Global-scale climate variability is often characterized by fluctuations in sea surface temperatures (SST), sea level pressures (SLP), geo-potential heights, wind speed, and other atmospheric-oceanic variables (Ghil, 2002).

There are several quasi-periodic atmospheric-oceanic oscillations that have teleconnection patterns with climate variability across the western United States. Two of the most prominent oscillations and foci of this study are the El Niño-Southern Oscillation (ENSO) and Pacific Decadal Oscillation (PDO). ENSO and PDO have quasi-periodic oscillations over 2-7 years and 15-35 years, respectively (Ghil, 2002; Kuss and Gurdak, 2014; Mantua and Hare, 2002). Common indices that are used to characterize these oscillations are the Multivariate ENSO Index (MEI) and Pacific Decadal Oscillation (PDO) Index (Figure 1ab).

Previous research has demonstrated that the interannual variability of ENSO and decadal to multidecadal variability of PDO may have different teleconnections to the terrestrial hydrologic processes that can affect groundwater budgets (e.g., Corona et al., 2018; Gurdak et al., 2007; Hanson et al., 2004; Kuss and Gurdak, 2014). For example,

these teleconnection patterns may influence fluctuations in groundwater levels (Corona et al., 2018; Gurdak et al., 2007; Hanson et al., 2004; Kuss and Gurdak, 2014; Tremblay et al., 2011; Velasco et al., 2015). Kuss and Gurdak (2014) found that ENSO and PDO have a greater control on groundwater level variations across the U.S. than the Atlantic teleconnection patterns associated with the North Atlantic Oscillation (NAO) and Atlantic Multidecadal Oscillation (AMO). In particular, the positive phases of PDO were associated with increased wet conditions and therefore greater recharge fluxes in the western and central principal aquifers of the U.S. While some of these teleconnection patterns of climate variability and groundwater processes have been defined at the regional aquifer scale, understanding how these teleconnection patterns impact local scale groundwater budgets is not well defined.

1.2 The El Niño-Southern Oscillation

The El Niño-Southern Oscillation (ENSO) is a recurring climate pattern that occurs approximately 2-7 years over the Pacific Ocean and is characterized by anomalies in sea surface temperature (SST) and sea level pressures (SLP) in the equatorial Pacific Ocean (Hanson et al., 2004). ENSO is also a critical teleconnection pattern in the Pacific Ocean due to its high frequency, seasonal effects on weather, and global impact on average and extreme weather events (McCabe and Dettinger, 1999; Ropelewski and Halpert, 1987; Velasco et al., 2015). ENSO consists of two phases; a positive or warm phase known as El Niño and a negative or cool phase known as La Niña. The Multivariate ENSO index (MEI) characterizes the intensity and duration of the El Niño and La Niña phases (Figure 1a). The MEI is a comprehensive index of ENSO because it

is based on multiple variables of the Combined Oceanic-Atmospheric Dataset, and represents an average of SLP, zonal and meridional winds, SST, and total cloudiness in the equatorial Pacific Ocean (Wolter and Timlin, 2011). Positive values of the MEI correspond to positive phases of ENSO (El Niño) and negative values correspond to the negative phase of ENSO (La Niña) (NOAA, 2018). Generally, the Southwestern U.S. may experience above average winter precipitation and the Northwestern U.S. may experience more extreme dry conditions during the El Niño phase, which creates a shift in the jet stream resulting from warm waters of the equatorial Pacific Ocean migrating eastward (McCabe and Dettinger, 1999; Ropelewski and Halpert, 1987). The El Niño phase results in above average precipitation in California, whereas there are decreases in precipitation observed in the Pacific Northwest. During the La Niña phase, the Southwestern U.S. and California may experience drier than average conditions and the Northwestern U.S. may experience increases in average winter precipitation, which is due to cooler SSTs in the equatorial Pacific Ocean (Ropelewski and Halpert, 1987). These effects during El Niño and La Niña years contribute to a known “dipole” effect (Brown and Comrie, 2004b).

1.3 The Pacific Decadal Oscillation

The Pacific Decadal Oscillation (PDO) is also a recurring Pacific climate pattern that generally has similar teleconnections patterns as ENSO in terms of climate variability for the Western U.S., except that the PDO has a decadal to interdecadal periodicity (Kuss and Gurdak, 2014; Mantua and Hare, 2002; Velasco et al., 2015; Zhang et al., 1997). PDO has one main period of 15 to 35 years, with a secondary period of 50-

70 years. Like ENSO, PDO is characterized by climate anomalies of SST and SLP in the Northern Pacific Ocean. During the positive phase of PDO, SSTs are cooler than average temperatures on the western coast of the U.S. Cooler SSTs can lead to increases in winter precipitation for the southwestern U.S. and increased drought conditions in the northwestern U.S. During negative phases of PDO, SSTs are warmer than average and lead to the reverse observations creating a dipole effect in the climate (Hanson et al., 2004; Mantua and Hare, 2002; Velasco et al., 2015). These climate and oceanic anomalies are used to construct the PDO Index (Figure 1b) (NOAA 2019). Changes in phase can impact other Pacific teleconnection patterns, specifically ENSO. For example, during the positive phase of PDO, there is a greater probability of the occurrence of the positive phase of ENSO, and the same pattern is observed for the negative phase of PDO (Brown and Comrie, 2004a; Kuss and Gurdak, 2014). Additionally, if PDO and ENSO are aligned in phase, the observed effects from can be more extreme. For example, if PDO and ENSO are both in the positive phase, El Niño events may be more intense and areas such as California which are normally impacted by El Niño would observe wetter conditions. Conversely, if PDO and ENSO are both in the negative phase, areas that are impacted by La Niña events would experience more intense effects. During a La Niña year that is in phase with PDO, California may experience increased drier conditions whereas the Pacific Northwest may experience increased intensity in precipitation.

1.4 Study Area

The Tulelake Irrigation District (TID) is located approximately 150 miles northeast of Redding, California and within the Upper Klamath River watershed (Figure

2). The northern boundary of the TID is the Oregon-California state line and the southern boundary of the TID is located near the Lava Beds National Monument. The TID encompasses 96,000 acres and approximately 60,000 acres are used for agriculture (City of Tulelake, 2020). The two main aquifer units within the TID are the sedimentary aquifer and the deep volcanic aquifer. The sedimentary aquifer is primarily composed of basin-fill sediments that result in moderate yield due to low to moderate permeability. Underlying the sedimentary aquifer is the deep volcanic aquifer, which is comprised of highly permeably basaltic lava flows. Both units are saturated, however the deep volcanic aquifer is the primary aquifer that can support irrigation in the TID. Historically, the TID primarily relied on surface-water diversions from the Klamath River to irrigate crops. However, in recent years the TID has become increasingly reliant on groundwater pumping to supplement decreases in surface-water diversions (Pischel and Gannett, 2015). As a result, the California Department of Water Resources (CA DWR) has categorized the TID as a medium priority groundwater basin under SGMA. The medium prioritization is attributed to declines in long-term water-level hydrographs from wells, the relatively high percentage of irrigated lands within the TID, and the dependence upon groundwater supplies (CA DWR Basin Prioritization, 2019). Simulated water balance models indicate that the increases in groundwater pumping and drought conditions are resulting in overdraft groundwater conditions for the TID (Pishel and Gannett, 2015).

Additionally, the TID is located between the dipole of known hydroclimatologic effects from ENSO and PDO (Brown and Comrie, 2004b). For example, the positive (negative) phase of ENSO is associated with below (above) average winter precipitation

for Washington state and other parts of the Pacific Northwest, and above (below) average winter precipitation for southern California. Beebee and Manga (2004) found that PDO and ENSO were not highly correlated with respective positive and negative phases in southern and southeastern Oregon as compared to northern Pacific Northwest. The teleconnections between climate variability associated with ENSO and PDO and groundwater resources in the TID are not well defined. More broadly, there is a lack of published research linking global-scale climate variability and local- to basin-scale groundwater hydrology and corresponding implications for groundwater management. The future trends in many hydrologic processes, including recharge due to human-induced climate change can only be fully appreciated when combined with understanding of the overprinted global-scale climate variability (Corona et al., 2018).

1.5 Scope and Purpose

The purpose of this research is to fill knowledge gaps about how climate variability and climate change influences groundwater resources at the local-basin scale by focusing on the TID. To do this, I will first quantify the effects of interannual to multidecadal climate variability associated with ENSO and PDO on the temporal variability of precipitation, streamflow, and groundwater levels in the TID. Second, I will evaluate the role of local-scale hydrogeologic properties in affecting recharge response to climate variability and change. The role of hydrogeologic properties will be explored by evaluating the spatial patterns in groundwater level responses across the TID to natural climate perturbations and by evaluating recharge beneath the two main soil textures across the TID under historic and future climate projections. To meet these objectives, I

analyzed long-term hydrologic time series using Singular Spectral Analysis (SSA) and built HYDRUS-1D (Šimůnek et al., 2008) models for a crop type and a range of soil hydraulic properties representative of the TID to simulate how climate variability and change influences recharge rates. By answering these questions within the TID, this research will provide insight into the role of interannual to multidecadal climate variability and future climate change on sustainable groundwater management for other similar basins in California that must comply with SGMA or more broadly across the western U.S.

2.0 Methodology

2.1 Data Selection

There are two general types of data used in this study; observed and simulated. The observed data include precipitation, air temperature, streamflow discharge, groundwater elevations, depth to water levels, and climate indices that are calculated based on observed atmospheric and oceanic data (Table 1). The observed data were largely used to evaluate the influence of ENSO and PDO on historical variability of the climate and hydrologic variables, including recharge rates in the TID. The simulated data were generated from global climate models (GCMs) and HYDRUS-1D (Šimůnek et al., 2008) simulations and include historic and projected climate variables, such as precipitation, air temperature, and groundwater recharge rates. The simulated data were largely used to evaluate the influence of climate change on historical and projected recharge rates in the TID.

2.1.1 Observed Data

All observed datasets were obtained from public data repositories. Climate indices were obtained from the Earth System Research Laboratory, Physical Sciences Division of NOAA (NOAA, 2019). The MEI spans from 1950 to 2017, and the PDO index spans from 1854 to 2019 (Figure 1). Precipitation data was obtained from the Climate Data Online portal, National Centers for Environmental Information of NOAA (NOAA CDO, 2019). This data spans from 1932 to 2018 and was collected in the city of Tulelake, which is centered in the TID (Figure 2). The span of the dataset makes it a reasonable choice for identifying ENSO and PDO signals. Air temperature data was also obtained from the Climate Data Online portal, National Centers for Environmental Information of NOAA (NOAA CDO, 2019), and spans from 1932 and 2018. This weather station (Air Temperature (Tulelake), (GHCND:USC0049053) is located within the bounds of the Tulelake Irrigation District. One additional weather station is used to fill any data gaps in the Tulelake air temperature dataset and is located approximately 15 miles south of the City of Tulelake near the Lava Beds National Monument (Air Temperature (Lava Beds NM), GHCND:USC00044838) (Figure 2).

Streamflow discharge was obtained from a stream gauge on the Klamath River (USGS 11501000) that is monitored by the U.S. Geological Survey (USGS) in the National Water Information System (NWIS) (USGS NWIS). This stream gauge is located on the Sprague River near Chiloquin, Oregon, approximately 47 miles from the northern border of the TID (Figure 2). The discharge data spans from 1921 to 2018. As there are no measurements of surface-water flow in the TID, this location on the Sprague River

near Chiloquin is used to represent approximate variability in surface water inflows to the TID. This gauging station was selected because it is the closest station to the TID that is not affected by dam releases and thus represents natural stream discharge response to hydroclimatologic variability, as well as the climate near Chiloquin, Oregon is similar to what is observed in the TID.

Groundwater level data from several wells in the TID was compiled from the California State Groundwater Elevation Monitoring System (CASGEM) (CASGEM, 2019). The groundwater wells used for this study were selected based on the well use, the length of the dataset, the location in the TID, and whether or not by visual inspection the groundwater hydrographs were dominated by human pumping or record natural variability in water levels. Wells were excluded if their water-level hydrographs were dominated only by seasonal pumping and did not show natural variability in the water levels. Most wells excluded appear to be used for irrigated agriculture. Of the more than 10 CASGEM wells in the TID, only three wells had hydrographs that met the selection criteria and were used in subsequent analyses (Figure 2). The wells used in this study are summarized in Table 1.

2.1.2 Simulated Data

Simulated data includes the precipitation, temperature, wind speed, relative humidity, and solar radiation from the four GCMs (Cal-Adapt, 2020) that were used as input to the HYDRUS-1D (Šimůnek et al., 2008) model scenarios and the associated output data from the HYDRUS-1D simulations. The GCM data and HYDRUS-1D model scenarios are described in detail in section 2.4.1 of this thesis.

2.2 Time Series Analysis

Time series analysis was performed using the U.S. Geological Survey (USGS) Hydrologic and Climatic Analysis Toolkit (HydroClimATe) (Dickinson et al., 2014). HydroClimATe is a computer program that was developed by the USGS to analyze relationships between noisy hydrologic time-series data and variable climatic data. This program can be used to pre-process data and to perform spectral analysis such as Fourier transformations, Single Spectrum Analysis (SSA), correlation analysis, and to make future projections (Dickinson et al., 2014). In this study, HydroClimATe was used in the pre-processing of the data, performing SSA, and calculating lag correlations between time-series data sets.

2.2.1 Data Pre-Processing

Prior to statistical analysis, several pre-processing steps were used to remove anthropogenic signals from the time series datasets, following methods outlined by Kuss and Gurdak (2014) and Hanson et al. (2004). Preprocessing steps include interpolation, cumulative departure, detrending, and normalization (Dickinson et al., 2014).

Interpolation was used to estimate missing data gaps in the time series. Specifically, Interpolation is used to give each data set a uniform monthly time step through estimating values for months that may be missing data. After interpolation, a cumulative departure curve is calculated, which is the sum of the difference between consecutive values in the time series and the mean of the series.

Cumulative departure is calculated by:

$$CD = \sum(x_i - \bar{x}) \quad \text{Eq. 1}$$

where:

CD is the cumulative departure curve
 x_i is the value at time i
 \bar{x} is the mean of the series

The cumulative departure of the time series allows for seasonal processes such as precipitation to be compared against more persistent time series datasets such as groundwater elevations or climate oscillations. Next, the curve fitting method is used to detrend the cumulative departure series to remove non-climate signals that might be associated with human activity, such as long-term changes in groundwater pumping. A 3rd order polynomial was used for the curve fitting to represent the overall trend of the data. Residuals are then calculated as the difference between the cumulative departure series and the fitted 3rd-order polynomial trend line at each time t . The residuals represent the time series with the overall trend removed (Dickinson et al., 2014). Residuals are then standardized to create normalized departure series from the mean, which allows for statistical comparisons among different types of datasets. The normalized departure series is normally distributed and has a sample mean equal to zero and a sample standard deviation equal to one:

$$z_i = \frac{x_i - \bar{x}}{s} \quad \text{Eq. 2}$$

where:

z_i is the normalized variable
 x_i is the mean of the original series
 \bar{x} is the sample mean of the series
 s is the sample standard deviation

2.2.2 Singular Spectrum Analysis (SSA)

SSA is a nonparametric method of estimating spectral correlations in noisy time series that has been used widely in geophysical and hydroclimatology studies (Vautard et al., 1992). Here, SSA is used to detect quasi-periodic oscillations in interannual to multidecadal climate indices of ENSO and PDO and the hydrologic time series (Hanson et al., 2004; Kuss and Gurdak, 2014; Vautard et al., 1992). SSA is performed on the normalized departure series of each climate index, precipitation, streamflow discharge, and groundwater levels. SSA decomposes the original time series into independent reconstructed components (RCs) that are then analyzed in an oscillatory pattern. The sum of the RCs is equal to the original time series signal, and thus no information is lost during reconstruction (Ghil, 2002; Hanson et al., 2004).

To explain the SSA method, I present the following equations and descriptions that are outlined in Dickinson et al. (2014). SSA starts with utilizing a trajectory matrix X , which is composed of a series of windows of the time series that have a length of M . The dimensions of the trajectory matrix are M_T by N_T

where:

N_T is equal to $N-M+1$
 N is the number of timesteps in the series, and
 M_T is the embedding dimension of X .

Then, the covariance matrix (C) is constructed using:

$$C = \frac{D^T D}{N_T} \quad \text{Eq. 3}$$

where:

C is an M_T by N_T covariance matrix
 D^T is the transpose of X , and
 D is an M_T by N_T trajectory matrix.

As described in Dickinson et al. (2014), the eigenvectors and eigenvalues of C are then calculated. This is done through the analysis of the eigenvectors and values of C in the following form:

$$CE = \lambda E \quad \text{Eq. 4}$$

where:

E is an M_T by N_T matrix of the eigenvectors,
and
 λ is the vector of eigenvalues of length, M_T .

A matrix of the principle components (A), is obtained through projecting the eigenvector E onto the trajectory matrix D :

$$A = E^T D \quad \text{Eq. 5}$$

where:

E is an M_T by N_T matrix of the eigenvectors, and
 A is an M_T by N_T matrix of the principle components.

The RCs are then calculated from:

$$RC = \frac{1}{M_T} \sum_{k \in K} \sum_{j=L_t}^{U_t} A_k(t-j+1)E_k(j) \quad \text{Eq. 6}$$

where:

K is the set of eigenvectors that are used in the

reconstruction,
M_t is a normalization factor,
L_t is a bound of summation, and
U_t is a bound of summation.

The values of M_t , L_t , and U_t vary depending on the interval of the time series:

$$(M_t, L_t, U_t) = \left\{ \begin{array}{ll} \left(\frac{1}{t}, 1, t \right), & 1 \leq t \leq M_T - 1 \\ \left(\frac{1}{M_t}, 1, M_t \right), & M_T \leq t \leq N_T \\ \left(\frac{1}{N - t + 1}, t - N + M_T, M_T \right) & N_T + 1 \leq t \leq N \end{array} \right\} \quad \text{Eq. 7}$$

Most of the variance within each time series is typically found within the first 10 RCs (Hanson et al., 2004). These first 10 RCs also typically contain the statistically significant oscillatory patterns that may be associated with global-scale climate variability (Hanson et al., 2004). The Ghil and Mo significance test was used to determine which of the 10 RCs were statistically significant using a red-noise null hypothesis (Ghil and Mo, 1991). Using only the statistically significant RCs, a composite RC was then created and compared to periodicities that fall within the ranges of ENSO and PDO. The composite RCs are calculated by grouping and summing the statistically significant RCs across the following periods: 2-7 years (ENSO) and 15-35 years (PDO). The composite RCs with periodicities greater than 35 years are denoted here as >PDO, which is consistent with previous studies that identify >PDO as variability that may be associated with the Atlantic Multidecadal Oscillation (AMO) (Gurdak et al., 2007; Kuss and Gurdak, 2014). This method allows for the composite RCs to represent significant

oscillatory modes within the time series that are consistent with ENSO, PDO, and >PDO (Gurdak et al., 2007; Kuss and Gurdak, 2014; Hanson et al., 2004). The composite RCs with periods 2-7 years that are consistent with ENSO and with periods 15-35 years that are consistent with PDO are then carried forward for lag correlation analyses.

2.2.3 Lag Correlation

Lag correlations are used to quantify and understand responses between climate and hydrologic variables in the TID system. In general, lag correlations measure associations between two variables at different points in shifted time, which results in a calculated value as a lag correlation coefficient (Helsel and Hirsch, 2002). Methods from Kuss and Gurdak (2014) and Velasco et al. (2017) are used to calculate lag correlations for the hydrologic datasets using the RCs from the SSA. Prior to calculating lag correlation coefficients, explanatory and response composite RCs are truncated to have the same start and end date. For example, if a precipitation data set has a specific start and end date, the climate index would be partitioned to the same start and end date for analysis. HydroClimATe reports both forward and backward lags between two time-series; only the first 60 months (5 years) of forward lags were considered based on the previous work of Hanson et al. (2006, 2004). Correlation coefficients are calculated for each monthly time lag using a 95-percent confidence level. Coefficients above this level are considered statistically significant.

2.3 Spatial Variation Analysis

Based on prior correspondence, a goal of this research is to examine if there are statistically significant differences in observed groundwater levels in the TID.

Groundwater wells selected for this analysis (Table 1) are divided based on the cardinal quadrant in the TID. Groundwater wells are not available in the southwestern quadrant of the TID due to the presence of the Tulelake Sump (Figure 2). To evaluate variation in the groundwater levels in three groundwater wells that are spatially distributed across the TID, I used a variety of statistical testing in the JMP software (*JMP*, 2009). I used the Shapiro-Wilks normality test with an alpha (α) level of 0.05 to determine that the water levels from the three wells all have a non-normal distribution. Therefore, I used subsequent non-parametric tests with an α -level of 0.05 to determine differences in the datasets (Helsel and Hirsch, 2002).

2.4 Groundwater Recharge Analysis

2.4.1 HYDRUS-1D

I developed HYDRUS-1D models to simulate recharge rates in the TID under a range of soil and climate scenarios. HYDRUS-1D (Šimůnek et al., 2008) is a computer code that uses a finite element method to numerically solve the Richards' equation (Richards, 1931) for variably saturated flow in porous media:

$$\frac{\partial \theta}{\partial t} = \frac{\partial}{\partial z} \left[K(\theta) \left(\frac{\partial h}{\partial z} + 1 \right) \right] \quad \text{Eq. 8}$$

where:

- θ is the volumetric water content,
- h is the soil water pressure head,
- t is time at t ,
- z is the vertical space coordinate, and
- K is the hydraulic conductivity.

Several scenarios were applied to the HYDRUS-1D models to evaluate the influence of soil hydraulic properties, land use, and climate variability and change effects on historic and projected recharge rates in the TID. The model scenarios are described next.

Two model scenarios were used to test the influence of soil hydraulic properties on recharge rates in the TID. Each scenario is a single-layer profile of the vadose zone that represents average soil textures in the TID. The two soil textures are based on the STATSGO2/SSURGO soil survey data from the TID (USDA NRCS, 2009). From the soil surveys, I determined that the dominant soil types in the TID are the Tulebasin mucky silty clay loam (i.e., Tulebasin soil) and the Laki fine sandy loam (i.e., Laki soil), which account for approximately 42% and 9% of the study area, respectively (USDA NRCS, 2009) (Figure 3). Based on these two soil types, I selected hydraulic parameters for the HYDRUS-1D models using the Rosetta database. The Rosetta database is a software package that predicts soil hydraulic parameters using a neural network model of thousands of USDA samples of soil texture data (Schaap et al., 2001). The resulting Tulebasin soil consists of 50% clay, 20% silt, 30% sand, and the Laki soil consists of 20% clay, 50% silt, and 30% sand. These parameters are based on Table 19 in the USDA Soil Survey of the Butte Valley-Tulelake Area. Table 2 summarizes the input values for the soil textures used in the HYDRUS-1D model.

The model scenario represents the average irrigated agricultural lands of the TID. Cereal grains account for 35% of the total irrigated lands in the TID (TID WMP, 2011).

The land use corresponds to a net irrigation requirement of 20 inches of water, or 38,665 Acre-feet per irrigation season, which spans from May through September.

The model scenarios that I used to test the influence of climate change on recharge rates in the TID are based on historic and future projections from four GCMs using the representative concentration pathways (RCP) of 4.5 and 8.5 (Cal-Adapt, 2020). The climate projections for historical data and RCP 4.5 and RCP 8.5 are: CNRM-CM5, CanESM2, HadGEM2-ES, and MIROC5. I used these four GCMs because the California Department of Water Resources (DWR) has recommended them for water related planning and management in California (Lynn et al., 2015). The GCM datasets were spatially downscaled using the Localized Construction Analog (LOCA) framework for California (Pierce et al., 2014). The historic data from the GCMs spans from 1950 to 2006 and the projected output from the GCMs span from 2006 to 2099. The historic and project GCM output is used as input to drive the HYDRUS-1D (Šimůnek et al., 2008) simulations. Output data that is generated from the HYDRUS-1D simulations spans from 1950 to 2099.

For all previously described model scenarios, the model domain was a 200-cm column that represents land surface to the average depth to groundwater of the TID. The 200-cm depth to water was determined from TID well logs from CASGEM. The HYDRUS-1D model accounts for root water uptake, which would represent agricultural coverage across the TID. The root zone is distributed in the upper 60 cm of the soil column, and root water uptake is calculated based on the Feddes model (Feddes et al., 1978). The model was discretized using a finite element size of 2.0 cm. Each model had

on average 100 nodes. Models were run at a daily time interval to capture smaller variations in groundwater recharge from 1950-2099.

For initial model conditions, a pressure head of 100 cm was applied throughout the soil column, which is based on methods from Rassam et al. (2018). An atmospheric boundary condition with surface runoff is applied at the upper boundary of the soil profile, and the lower boundary condition is simulated as free drainage to calculate the bottom flux of the soil profile. In addition to the atmospheric upper boundary condition, irrigation is also applied to only the irrigated agricultural model scenarios. Based on the irrigation requirements and crop coverage for cereal grains in the TID Water Management Plan (TID WMP, 2011), an irrigation rate of 0.341 cm per day is applied annually only during the irrigation season between May to September.

2.4.2 Model Calibration

Previous estimates of groundwater recharge in the TID have ranged from about 75 to 300 mm/year (Pishel and Gannett, 2015). Recharge in the alluvial aquifer is primarily sourced from applied irrigation water and canal leakage accounting for larger percentages of groundwater recharge around the TID, and precipitation is only accounting for a small percentage as compared to other sources of recharge (Pishel and Gannett, 2015). In order to appropriately analyze how precipitation may influence groundwater recharge in the TID, recharge values are compared to modeled literature values for the TID (Pishel and Gannett, 2015).

3.0 Results and Discussion

3.1 Variance of Climate Variability in Hydrologic Time Series

The SSA results indicate that there are statistically significant composite RCs in the precipitation, streamflow, and groundwater level time series that can be attributed to ENSO, PDO, and >PDO (Table 3). The majority of the variance in the precipitation time series was attributed to >PDO and PDO, capturing 42% and 37% of the percent variance, respectively (Table 3). The >PDO RC in the precipitation had a period of 43.5 years (Table 3). Only 8.3% of the percent variance in the precipitation time series is attributed to ENSO, which indicates the importance of the lower-frequency climate forcings, with lesser control by ENSO on precipitation variability in the TID. The majority of the variance in the streamflow was also dominated by the lower-frequency climate forcings, with 93% of the percent variance attributed to >PDO with a period of 99.1 years (Table 3). However, the PDO only accounts for 6% of the percent variance in the streamflow, which is a considerably lower relative percent variance as compared to the precipitation time series. The RCs consistent with ENSO account for only 0.3% of the percent variance in the streamflow time series (Table 3).

Although the SSA results indicate that the inflows (precipitation and streamflow) to the groundwater system are most influenced by the >PDO and PDO variability, the three groundwater levels in the TID did not contain RCs with periods consistent with >PDO (Table 3). The lack of RCs consistent with >PDO in the groundwater levels may be attributed to the relatively short length of records (<20 years) for the three wells as compared to the precipitation and streamflow time series (Table 1). However, the

majority of the variance in the three groundwater levels was attributed to PDO, capturing between 61 and 94% of the percent variance in the three wells (Table 3). While one well (Groundwater (NW)) did not contain RCs consistent with ENSO, the two other wells had water levels with 15 to 26% of the percent variance attributed to ENSO (Table 3).

The SSA results of relatively larger contribution of PDO-like than ENSO-like variability in the groundwater levels is generally consistent with previous studies (Gurdak et al., 2007, Kuss and Gurdak, 2014; and Velasco et al., 2015). These studies found that the lower frequency climate oscillations generally contain most of the variance in the groundwater level time series when compared to higher frequency oscillations. The detection of ENSO-like and PDO-like variability in the groundwater levels is also consistent with the damping depth framework presented by Corona et al. (2018) that can be used to explain why some periodic infiltration fluxes associated with climate variability dampen with depth in the vadose zone and are not detected in groundwater levels. By applying the semi-arid climate and relatively shallow (<4 m) depths to water of the TID within the damping depth framework (Figure 4 from Corona et al., 2018), both ENSO- and PDO-like fluctuations in land surface fluxes are theoretically expected to propagate through the vadose zone and be detected in the water- level fluctuations at all three wells sites in the TID. While all three groundwater levels have PDO-like variability, it is unclear why only two of the three wells have ENSO-like variability in the water level. I hypothesize that the lack of ENSO-like variability at groundwater (NW) well (Groundwater NW, Table 1) might be attributed to local-scale variations or layering in the hydrogeologic properties that affect the recharge fluxes in the vadose zone.

3.2 Lag Correlation

Lag correlation results are presented based on each variable (climate index, precipitation, streamflow, and groundwater) (Table 4). The climate indices for ENSO and PDO are considered as the independent variable and are related to the dependent variables of inflows (precipitation and streamflow) and groundwater levels (Table 4).

3.2.1 Climate

Results for the lag correlations between PDO and hydrologic inflows and groundwater levels are shown in Table 4 and Figure 4a. Results for lag correlations between ENSO and associated data are shown in Table 4 and Figure 4b. Climate-precipitation lag correlations resulted in higher minimum and maximum correlation coefficients on average for the PDO correlations as compared to the ENSO correlations (Table 4, Figure 4a). Although higher correlation coefficients are obtained for PDO, average correlation coefficients for ENSO with hydrologic time series have a non-significant correlation values (-0.003 to -0.066) and an average lag time ranging from 1.3 to 3.6 years (Table 4).

The results of the lag correlations between climate indices and precipitation have a positive relation between the ENSO and PDO and precipitation during the first lag year, which is the typical timeframe that precipitation in California responds to changes in the ENSO and PDO (Table 4, Figure 4ab). PDO had the higher maximum correlation to precipitation with a maximum value of 0.59 and a lag of 1.3 years, which was the highest of any hydrologic inflow and climate. Precipitation has a maximum correlation with ENSO of 0.29 and a lag of approximately 0.25 years (Table 4, Figure 5).

Streamflow lag correlations between climate indices and streamflow have an inverse relation between PDO during the first 5-lag years, whereas the streamflow lag correlation between ENSO have a positive relation during the first lag year (Figure 4b, Table 4). PDO and streamflow had a maximum lag correlation of -0.28 with no corresponding lag time (Figure 4a, Table 4). ENSO and streamflow discharge correlations had a maximum value 0.24 with a lag of 5 years (Table 4). The average correlation value between ENSO and streamflow discharge is -0.039 which has a corresponding lag time of 3.6 years (Table 4). The marginally statistically significant correlations to ENSO may indicate that the location of the gauging station may be located outside the known areas affected by the ENSO “dipole” (Beebee and Manga et al., 2004). Moreover, the location of the gauging station further north than the irrigation district (Figure 2), which is further outside the known areas affected by the ENSO “dipole. Additionally, the lack of positive correlations to PDO suggests that the watershed response to climate variability is complex and may be influenced by other controls on discharge such as snowmelt, or human-controlled factors (e.g., timing and magnitude of scheduled dam releases).

Groundwater level lag correlations with climate indices were not conclusive and did not show an obvious relation (Table 4, Figure 4ab). Groundwater levels in the northwestern area of the TID have a negative relation with PDO for the approximately first two lag years, whereas groundwater levels in the southeastern area of the TID have a positive relation with PDO for approximately the first 4 lag years (Figure 4a). Groundwater level lag correlations have a similar pattern in the northeastern and

southeastern groundwater wells when compared with ENSO (Figure 4b). Groundwater levels in the northeastern area of the TID have strong correlations (0.50) with ENSO with lag times corresponding to 3.5 years (Figure 4b, Table 4). Lag correlations for the southeastern groundwater well and ENSO have a strong correlation of 0.59 at a lag time of 2.8 years (Figure 4b, Table 4). When comparing to ENSO, groundwater level correlations peak 1 to 3 years after precipitation correlations peak. Such trends could be associated with hydrologic processes and infiltration through the vadose zone.

3.3 Spatial Variation in Groundwater Levels in the Tulelake Irrigation District

Understanding how temporal climate variability may influence the spatial patterns of groundwater level variability is important. Based on personal communication with TID Manager Brad Kirby, there appear to be spatial patterns in how some TID groundwater levels respond during the same time periods. These spatial patterns in groundwater level responses could be related to differences in local scale hydrogeologic properties and/or water budget stresses (pumping or recharge) across the TID. While there is some moderate variation in the soils across the TID (Figure 3), the well completion reports from the CASGEM wells indicated little variability in the vertical stratification of hydrogeologic properties, particularly within the vadose zone and near the regional water table.

The results of the Shapiro-Wilks normality tests (α -level = 0.05) indicate that the depth to water from the three wells are not normally distributed (Figure 5). The northeastern well are not normally distributed (p-value = <0.0001) and are right skewed, whereas the southeastern well is not normally distributed (p-value = <0.0001) and left

skewed. The northwestern well are not normally distributed (p-value = <0.0001) but do not illustrate clear left or right skewness. The results of the Kruskal-Wallis test (p-value = <0.0001 , $\alpha = 0.05$) indicate that there are statistically significant differences between the depth to water in the three wells spatially distributed across the TID (Figure 5). This difference can be due to a variety of factors including local geology, soil textures, hydraulic connectivity to the local aquifer, or well depth.

When comparing the local soil texture observed near the wells to see if differences in soil texture may be influencing the different depth to water measurements, there are three soil types located around the wells: the Tulebasin clay in the northwest, the Laki sandy loam in the northeast, and the Strukel sandy loam in the southeast (Figure 3). The two northern wells have less variability in the depth to water measurements than the southern well (Figure 5). The northwestern well has average depth to water measurements are 11.9 feet, with a range of 8 to 16 feet, whereas the northeastern well has more variability and has average depth to water measurements that are 12.3 feet, and have a range of 9 to 22 feet. (Figure 5, Table 1). The results of the Kruskal-Wallis test (p-value = 0.0608, $\alpha = 0.05$) indicate that there are not statistically significant differences between the depth to water measurements of the two northern wells (Figure 5). When performing a similar comparison between the northeast and southeast well, which has a similar soil texture as the northeast well, statistically significant differences are detected between the depth to water measurements (p-value = <0.0001 , $\alpha = 0.05$). This difference in the northeast and southeast well may be attributed to difference in well depth as the southern well is finished deeper (83 ft. below ground surface) rather than the northeastern

well (38 feet below ground surface). Additionally, differences may also be due to factors such as connectivity to the local aquifer or hydrogeologic properties, or water use/pumping may be a more dominant factor on groundwater levels rather than soil textures.

3.4 Groundwater Recharge in Tulelake Irrigation District

This study simulated groundwater recharge using historic and future climate data from GCMs under RCPs 4.5 and 8.5. The results were then combined to show yearly simulated cumulative recharge in both the Tulebasin and Laki soil profiles. In order to evaluate how well the models were simulating groundwater recharge, comparisons were made between simulated recharge rates from the Hydrus-1D models and literature values ranging from about 75 to 300 mm per year (Pishel and Gannett, 2015).

3.4.1 Groundwater Recharge by Soil Texture

I simulated recharge beneath the Tulebasin and Laki soils using a combination of measured and modeled datasets. Recharge rates ranged from 0 to 450 mm per year beneath both soils (Figure 6). The median recharge beneath the Tulebasin and Laki soils was 143 and 141 mm per year, respectively (Figure 6). These recharge rates are within a reasonable range as reported for the TID in Pishel and Gannett (2015).

Results of the Wilcoxon test (α -level = 0.05) indicate that there are no statistical differences (p-value = 0.7078) in the annual recharge rates beneath each of the two soils over the period of 1950-2099 (Figure 6). The lack of statistical differences in annual recharge rates is further supported by the lack of statistical differences in depth to water

measurements (i.e., groundwater levels) in similar soil textures (Figure 6), which may be attributed to local processes such as groundwater pumping and/or use or differences in hydrogeologic properties, rather than local differences in soil texture.

3.4.2 Groundwater Recharge in the Tulelake Irrigation District by Time Period

Annual recharge was also evaluated for the same soil profiles under RCPs 4.5 and 8.5 (Figure 7). The time periods evaluated were: historic (1950-2005), present (2006-2039), near-future (2040-2069) and future (2070-2099). The greatest recharge rates are observed during the historical time period with median recharge rates of 181 mm/yr in the Tulelake sediments (Figure 7a) and 179 mm/yr in the Laki sediments (Figure 7b). For both soils, the lowest simulated annual recharge is during the future time period (Figure 7). Based on the results from the Steel-Dwass test (α -level = 0.05), there are statistically significant differences for each time period when compared to the historic time period (p-values = <0.0001). Under both RCPs and soil types, the median annual recharge declines by 51% between the historical (median = 179 to 181 mm/yr) and future (median = 77 to 99 mm/yr) periods (Figure 7). However, there are no statistically significant differences (p-values = 0.983 to 1) in the annual recharge rates beneath RCP 4.5 and 8.5 for either the Tulelake or Laki soils (Figure 7). While the results of the simulated annual recharge indicate a statistically significant reduction between the historical period to the end of the 21st century, these simulated annual recharge rates are apparently insensitive to differences in the RCP 4.5 and 8.5 scenarios. The large reduction in annual recharge could have important implications for the groundwater budget and sustainable management practices in the TID during the coming decades of the 21st century. Next, I

explore the causes for the simulated decline in future recharge as a response to projected precipitation, temperature, and evapotranspiration.

The projected annual precipitation under RCP 4.5 has a non-significant (p-values = 0.9875 to 1) increase in median values during the three time periods of the 21st century (Figure 8). Under RCP 8.5, the projected annual precipitation median values also increase during the 21st century, but only the future period has statistically significant (p-value = 0.0026) and greater precipitation compared to the historic period (Figure 8). During the future time period, the RCP 8.5 scenario (median = 322 mm) forecasts nearly 10% greater annual precipitation than the RCP 4.5 scenario (median = 293 mm) (Figure 8).

The projected temperature under RCP 4.5 has a statistically significant increase during each of the three time periods of the 21st century, with temperatures peaking in the future time period (Figure 9). Unlike the projected precipitation, there are statistically significant differences in the projected temperature under both RCP 4.5 and 8.5 between the historic to the present (p-value = <0.0001), historic to near future (p-value = <0.0001), and historic to future time periods (p-value = <0.0001) (Figure 9). The RCP 8.5 scenarios result in statistically significant (p-value = <0.0001) and greater temperatures than the corresponding RCP 4.5 scenarios during the near future (13% greater average temperatures) and future (33% greater average temperatures) periods (Figure 9). The RCP 4.5 scenario has a global temperature that peaks and stabilizes within the near future period, while the RCP 8.5 scenario has a global temperature that peaks in the future period. Both RCP 4.5 and 8.5 scenarios are reflected in the downscaled temperature trends of the TID study area (Figure 9).

Simulated evapotranspiration increases continuously under both RCP 4.5 and 8.5 (Figure 10). The highest evapotranspiration rates are simulated during the future time period with median evapotranspiration rates ranging from 1.50 to 1.68 mm per day for both RCPs 4.5 and 8.5, respectively (Figure 10). Based on the results from the Steel-Dwass test (α -level = 0.05), there are statistically significant differences for each time periods when compared to the historic time period (p-values = <0.0001). Under both RCPs, evapotranspiration rates increase by approximately 25% between the historic (median = 1.27 mm/day) and future time periods (1.501 to 1.683 mm/day), RCP 4.5 and RCP 8.5 respectively. There are no statistically significant differences (p-value = 0.9975) in simulated evapotranspiration rates under RCP 4.5 when compared to RCP 8.5 (Figure 10). The continuous increases in evapotranspiration rates across the future time periods have a positive relation with temperature with increases in temperature corresponding to increases in evapotranspiration rates (Figure 9 and 10).

When comparing trends in precipitation and temperature to groundwater recharge, similar trends are noted under RCP 4.5 as RCP 8.5. In the RCP 4.5 scenario, significant decreases in annual recharge rates are the result of significant increases in temperature values and evapotranspiration rates (Figure 7, 9, 10). Similar trends that are noted under RCP 4.5 are also reflected in the RCP 8.5 simulations (Figure 7, 9, 10). In both scenarios, the trends between temperature, evapotranspiration rate, and annual recharge rates indicate that future recharge rates are relatively more sensitive to changes in temperature and evapotranspiration, rather than precipitation. Moreover, this relationship between groundwater recharge, temperature, and evapotranspiration is supported through the

presence of a shallow water table (<4 m), which can result in groundwater levels having a dynamic response to climate stressors (i.e., changes in air temperature).

4.0 Conclusion

The climate variability modes of >PDO, PDO and ENSO were shown to have moderate to strong influence on hydrologic variables in the TID, based on results of the SSA and lag correlations. While PDO accounted for the greatest amount of variance in the hydrologic time series, groundwater levels in the northeast and southeast areas of the TID were moderately correlated with ENSO and PDO.

Results of the non-parametric statistical testing indicate that there are not statistical differences between depth to water measurements (i.e., groundwater levels) in three spatially distributed wells across the TID. This is further verified when comparing the northern wells, which have local sediments consistent with the two most common sediments in the TID (Tulebasin clay and Laki sandy loam). The non-parametric statistical testing also indicates that there are no differences between depth to water measurements in the northern wells. When examining the northeastern depth to water values (Laki sandy loam) and the southeastern depth to water values (Strukel sandy loam), which are of similar soil textures, statistical testing indicates that there are statistical differences between the wells. This variation in statistical results indicate that differences may be due to factors such as connectivity to the local aquifer and water use/pumping rather than local geology or soil textures.

I used HYDRUS-1D models to simulate groundwater recharge from 1950 to 2099 under historic and future conditions using downscaled output from GCMs and RCP 4.5 and 8.5. Homogeneous models are representative of the two most common soil textures in the TID (Tulebasin and Laki soils) and recharge rates are quantified to determine if there are differences between recharge rates under each soil. Additionally, the Tulebasin and Laki soil profiles are analyzed during historic, present, near future, and future to assess how recharge will vary over time in relation to climate change.

Overall, there are no statistically significant differences in simulated recharge when comparing the Tulebasin and Laki sediments. When comparing simulated recharge across the modeled time periods, the future time period had the lowest recharge rates ranging from 81 to 97 mm per year for the Tulebasin sediment, and from 77 to 93 mm per year for the Laki sediment under both the RCP 4.5 and 8.5. The historic time period had the highest recharge rates, which ranged from 179 to 182 mm per year for the both soils and RCPs. The recharge rates during all time periods are consistent with previous estimates of groundwater recharge in the TID (Pishel and Gannett, 2015).

Both RCP 4.5 and 8.5 simulations had statistically significant decreases in recharge from the historic to future time periods. Moreover, these statistically significant decreases in recharge are the result of statistically significant increases in air temperature and simulated evapotranspiration for both RCP 4.5 and 8.5. Observed trends between simulated recharge, air temperature, and evapotranspiration may indicate that the shallow vadose zone (<4 m) provides a dynamic response to climate with temperature as the dominant climatic control on groundwater recharge.

The findings from this study can be used to understand how interannual to multidecadal climate variability may influence local-scale groundwater resources in this region in California. Understanding how water resources may change during periods of climate variability may provide a pathway to understand how water resources may respond to the impacts of climate change. By understanding how recharge may vary spatially in the TID under climate change, water managers may be able to adapt more appropriately to focus groundwater replenishment efforts in areas that have favorable recharge rates. Additionally, the methods implemented in this research can provide a framework for examining how climate change may influence and impact management scale groundwater resources.

5.0 References

- Beebee, R.A., Manga, M., 2004. Variation in the relationship between snowmelt runoff in Oregon and ENSO and PDO. *Journal of the American Water Resources Association* 40, 1011–1024.
- Brown, D.P., Comrie, A., 2004. A winter precipitation “dipole” in the western United States associated with multidecadal ENSO variability. *Geophysical Research Letters* 31.
- California Department of Water Resources, 2017. Sustainable Groundwater Management
- California Department of Water Resources, 2019. Final Groundwater Basin Prioritization.
- City of Tulelake, 2020. About Tulelake, City of Tulelake, California.
- Corona, C.R., Gurdak, J.J., Dickinson, J.E., Ferré, T.P.A., Maurer, E.P., 2018. Climate variability and vadose zone controls on damping of transient recharge. *Journal of Hydrology* 561, 1094–1104. <https://doi.org/10.1016/j.jhydrol.2017.08.028>
- Cal-Adapt, 2020. LOCA Downscaled CMIP5 Climate projections. <https://cal-adapt.org/data/download/>
- Dickinson, J.E., Hanson, R.T., Predmore, S.K., 2014. HydroClimATe—Hydrologic and Climatic Analysis Toolkit, in: *Hydrologic Analysis and Interpretation, Techniques and Methods*. U.S. Geological Survey, Reston, Virginia, p. 48.
- Feddes, R.A., Kowalik, P.J., Zaradny, H., 1978. Simulation of field water use and crop yield, *Simulation monographs*. Wiley, New York.
- Famiglietti, J.S., 2014. The global groundwater crisis. *Nature Climate Change* 4, 945–948. <https://doi.org/10.1038/nclimate2425>
- Ghil, M., 2002. Natural Climate Variability, in: *Encyclopedia of Global Environmental Change, The Earth System: Physical and Chemical Dimensions of Global Environmental Change*. Wiley, Chichester ; New York, p. 6.
- Ghil, M., Mo, K.T., 1991. Intraseasonal Oscillations in the Global Atmosphere. *Journal of the Atmospheric Sciences* 48, 752–790.
- Green, T.R., Taniguchi, M., Kooi, H., Gurdak, J.J., Allen, D.M., Hiscock, K.M., Treidel, H., Aureli, A., 2011. Beneath the surface of global change: Impacts of climate

change on groundwater. *Journal of Hydrology* 405, 532–560.
<https://doi.org/10.1016/j.jhydrol.2011.05.002>

Gurdak, J.J., Hanson, R.T., McMahon, P.B., Bruce, B.W., McCray, J.E., Thyne, G.D., Reedy, R.C., 2007. Climate variability controls on unsaturated water and chemical movement, High Plains aquifer, USA. *Vadose Zone Journal* 6, 533.
<https://doi.org/10.2136/vzj2006.0087>

Hanson, R.T., Newhouse, M.W., Dettinger, M.D., 2004. A methodology to assess relations between climatic variability and variations in hydrologic time series in the southwestern United States. *Journal of Hydrology* 287, 252–269.
<https://doi.org/10.1016/j.jhydrol.2003.10.006>

Helsel, D.R., Hirsch, R.M., 2002. Chapter A3: Statistical Methods in Water Resources, in: *Techniques of Water Resources Investigations, Book 4*. U.S. Geological Survey, p. 522.

JMP: release 8, 2nd ed. ed, 2009. . SAS Institute Inc, Cary, N.C.

Kuss, A.J.M., Gurdak, J.J., 2014. Groundwater level response in U.S. principal aquifers to ENSO, NAO, PDO, and AMO. *Journal of Hydrology* 519, 1939–1952.
<https://doi.org/10.1016/j.jhydrol.2014.09.069>

Lauffenburger, Z.H., Gurdak, J.J., Hobza, C., Woodward, D., Wolf, C., 2018. Irrigated agriculture and future climate change effects on groundwater recharge, northern High Plains aquifer, USA. *Agricultural Water Management* 204, 69–80.
<https://doi.org/10.1016/j.agwat.2018.03.022>

Mantua, N.J., Hare, S.R., 2002. The Pacific Decadal Oscillation. *Journal of Oceanography* 58, 35–44.

McCabe, G.J., Dettinger, M.D., 1999. Decadal variations in the strength of ENSO teleconnections with precipitation in the western United States. *International Journal of Climatology* 19, 1399–1410.

Meixner, T., Manning, A.H., Stonestrom, D.A., Allen, D.M., Ajami, H., Blasch, K.W., Brookfield, A.E., Castro, C.L., Clark, J.F., Gochis, D.J., Flint, A.L., Neff, K.L., Niraula, R., Rodell, M., Scanlon, B.R., Singha, K., Walvoord, M.A., 2016. Implications of projected climate change for groundwater recharge in the western United States. *Journal of Hydrology* 534, 124–138.
<https://doi.org/10.1016/j.jhydrol.2015.12.027>

NOAA CDO, 2019. Climate Data Online.

NOAA ESRL, 2019. Physical Sciences Division.

Pierce, D.W., Cayan, D.R., Thrasher, B.L., 2014. Statistical Downscaling Using Localized Constructed Analogs (LOCA). *J. Hydrometeor.* 15, 2558–2585. <https://doi.org/10.1175/JHM-D-14-0082.1>

Pishel, E.M., Gannett, M.W., 2015. Effects of groundwater pumping on agricultural drains in the Tule Lake subbasin, Oregon and California: U.S. Geological Survey Scientific Investigations Report 2015–5087 (Scientific Investigations Report No. 5087). U. S. Geological Survey.

Rassam, D., Šimůnek, J., Mallants, D., Van Genuchten, M.T., 2018. The HYDRUS-1D Software Package for Simulating the Movement of Water, Heat, and Multiple Solutes in Variably Saturated Media: Tutorial, Version 1.00. CSIRO Land and Water, Australia.

Richards, L., 1931. Capillary conduction of liquids in porous mediums. *Physics* 1, 318–333.

Ropelewski, C.F., Halpert, M.S., 1987. Global and regional scale precipitation patterns associated with the El Niño/Southern Oscillation. *Monthly Weather Review* 115, 1606–1626.

Schaap, M.G., Leij, F.J., van Genuchten, M.T., 2001. ROSETTA: a computer program for estimating soil hydraulic parameters with hierarchical pedotransfer functions. *Journal of hydrology* 251, 163–176.

Šimůnek, J., van Genuchten, M.Th., Šejna, M., 2008. Development and Applications of the HYDRUS and STANMOD Software Packages and Related Codes. *Vadose Zone Journal* 7, 587–600. <https://doi.org/10.2136/vzj2007.0077>

Taylor, R.G., Scanlon, B., Döll, P., Rodell, M., van Beek, R., Wada, Y., Longuevergne, L., Leblanc, M., Famiglietti, J.S., Edmunds, M., Konikow, L., Green, T.R., Chen, J., Taniguchi, M., Bierkens, M.F.P., MacDonald, A., Fan, Y., Maxwell, R.M., Yechieli, Y., Gurdak, J.J., Allen, D.M., Shamsudduha, M., Hiscock, K., Yeh, P.J.-F., Holman, I., Treidel, H., 2013. Ground water and climate change. *Nature Climate Change* 3, 322–329. <https://doi.org/10.1038/nclimate1744>

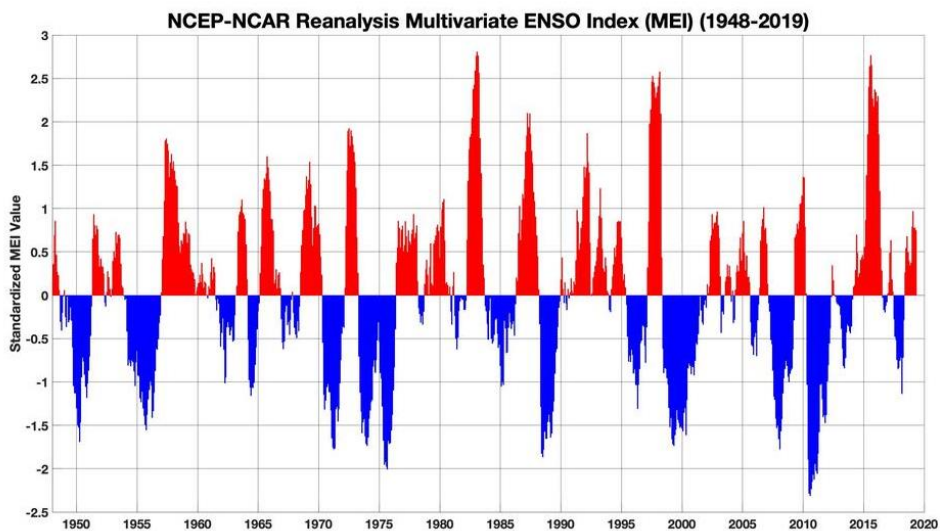
Tremblay, L., Larocque, M., Anctil, F., Rivard, C., 2011. Teleconnections and interannual variability in Canadian groundwater levels. *Journal of Hydrology* 410, 178–188. <https://doi.org/10.1016/j.jhydrol.2011.09.013>

Tulelake Irrigation District, 2011. Water Management Plan-Draft.

- USDA NRCS, 2009. Hydrologic Soil Groups, in: National Engineering Handbook Part 630 Hydrology. U.S. Department of Agriculture, Natural Resources Conservation Service, p. 14.
- Vautard, R., Pascal, Y., Ghil, M., 1992. Singular Spectrum Analysis: A toolkit for short, noisy, chaotic time series. *Physica D: Nonlinear Phenomena* 58, 95–126.
- Velasco, E.M., Gurdak, J.J., Dickinson, J.E., Ferré, T.P.A., Corona, C.R., 2015. Interannual to multidecadal climate forcings on groundwater resources of the U.S. West Coast. *Journal of Hydrology: Regional Studies*. <https://doi.org/10.1016/j.ejrh.2015.11.018>
- Wolter, K., Timlin, M.S., 2011. El Niño/Southern Oscillation behaviour since 1871 as diagnosed in an extended multivariate ENSO index. *International Journal of Climatology* 31, 1074–1087. <https://doi.org/10.1002/joc.2336>
- Zhang, Y., Wallace, J.M., Battisti, D.S., 1997. ENSO-like interdecadal variability: 1900–93. *Journal of climate* 10, 1004–1020.

6.0 Figures

(a)



(b)

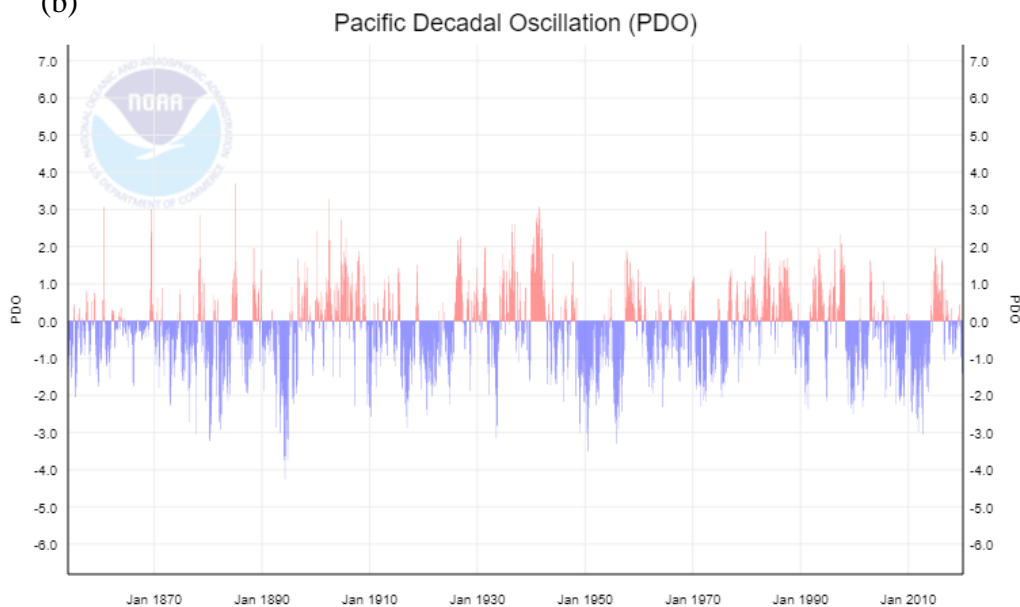


Figure 1: (a) The Multivariate ENSO Index (MEI) on a monthly timescale from 1950 to 2019 (NOAA, 2019). (b) The Pacific Decadal Oscillation Index on a monthly timescale from 1900 through 2017 (NOAA, 2018).

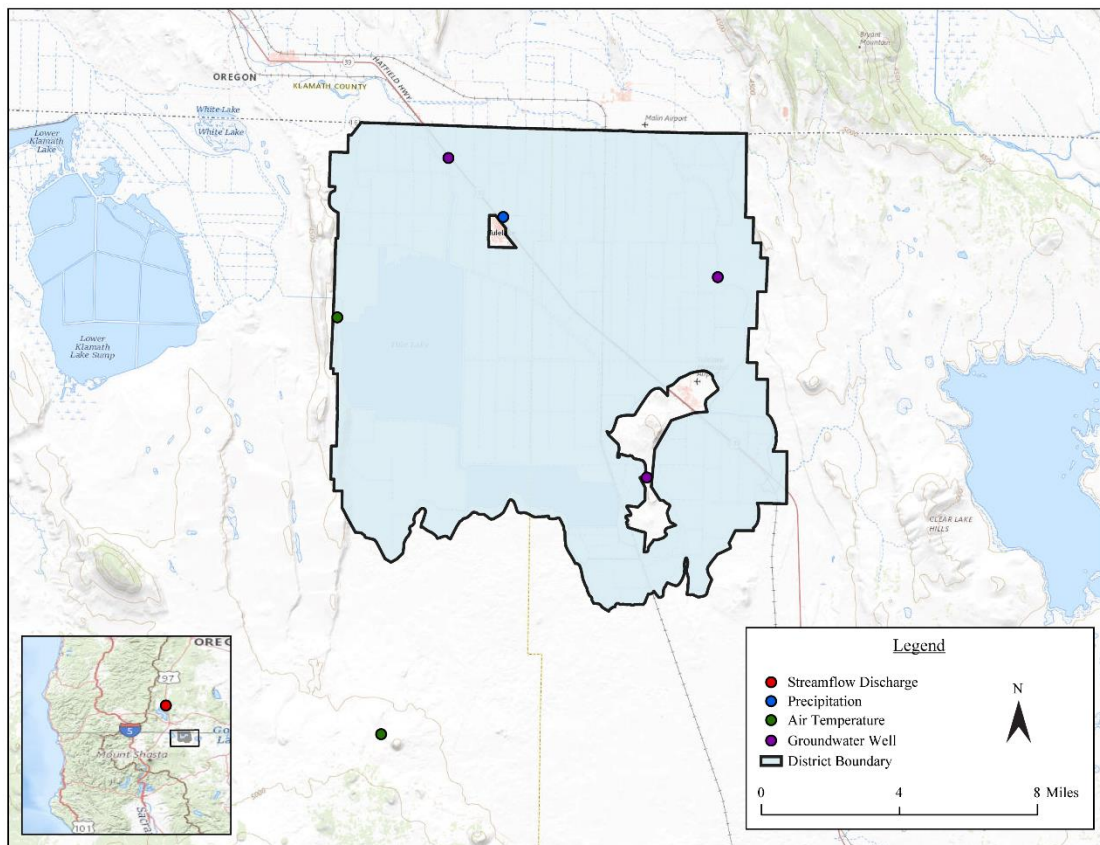
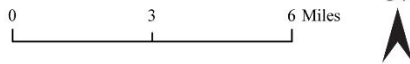


Figure 2: Map of the Tulelake Irrigation District, Tulelake, California. Groundwater wells used for analysis are denoted as purple circles. Weather stations used for climatic data sets are precipitation (blue circle) and temperature (green circles). The stream gage station (red circle) is on the Sprague River in Oregon (see map inset).

Soil Map of the Tulelake Irrigation District, Tulelake, CA

Soil Legend	
Capjac silt loam, 0 to 1 percent slopes	Rejo sandy loam, 0 to 2 percent slopes
Capjac silt loam, ponded, 0 to 1 percent slopes	Rejo sandy loam, 2 to 9 percent slopes
Capona cobbly loam, 5 to 30 percent slopes	Rubbleland
Capona-Rock outcrop complex, 0 to 5 percent slopes	Salisbury-Debar complex, 0 to 9 percent slopes
Dehill fine sandy loam, 0 to 5 percent slopes	Searles variant very stony loam, 0 to 5 percent slopes
Dehill fine sandy loam, 5 to 15 percent slopes	Searles-Truax-Orhood complex, 2 to 15 percent slopes
Demox stony sandy loam, 2 to 15 percent slopes	
Demax-Rubbleland complex, 15 to 50 percent slopes	
Dotia sandy loam, 0 to 5 percent slopes, MLRA 21	
Forchey loamy fine sand, 0 to 2 percent slopes, north, MLRA 21	
Forchey loamy fine sand, 0 to 2 percent slopes, south, MLRA 21	
Forchey loamy fine sand, 5 to 15 percent slopes	
Forchey loamy fine sand, slightly wet, 0 to 2 percent slopes, MLRA 21	
Fredotyer-Rock outcrop complex, 30 to 50 percent slopes	Stukel sandy loam, 5 to 30 percent slopes
Karac-Rock outcrop complex, 50 to 75 percent slopes	Stukel-Capona complex, 2 to 30 percent slopes
Laki fine sandy loam, 0 to 2 percent slopes	Truax fine sandy loam, 0 to 5 percent slopes
Laki-Henley complex, 0 to 2 percent slopes, MLRA 21	Truax-Searles, 2 to 9 percent slopes
Lamath silt loam, 0 to 1 percent slopes	Tulana silt loam, 0 to 1 percent slopes
Leavers sandy loam, drained, 0 to 5 percent slopes	Tulebasin mucky silty clay loam
Lequieu very stony loam, 0 to 2 percent slopes	Water
Lequieu-Adieux complex, 0 to 5 percent slopes	Zambar sandy loam, 0 to 2 percent slopes
Midoc loam, 0 to 2 percent slopes	Zuman loamy fine sand, 0 to 1 percent slopes
Midoc loam, bedrock substratum, 2 to 5 percent slopes	
Munnell gravelly loam, 0 to 5 percent slopes	
Pit silty clay, 0 to 2 percent slopes	
Podus loamy fine sand, 0 to 2 percent slopes, MLRA 21	
Poc loamy fine sand, 0 to 2 percent slopes	
Pomari loamy sand, 0 to 2 percent slopes	



Soil Survey Staff, Natural Resources Conservation Service, United States Department of Agriculture. U.S. General Soil Map (STATSGO2). Available online at <https://sdmdataaccess.sc.egov.usda.gov>.
 Soil Survey Staff, Natural Resources Conservation Service, United States Department of Agriculture. Soil Survey Geographic (SSURGO) Database. Available online at <https://sdmdataaccess.sc.egov.usda.gov>.

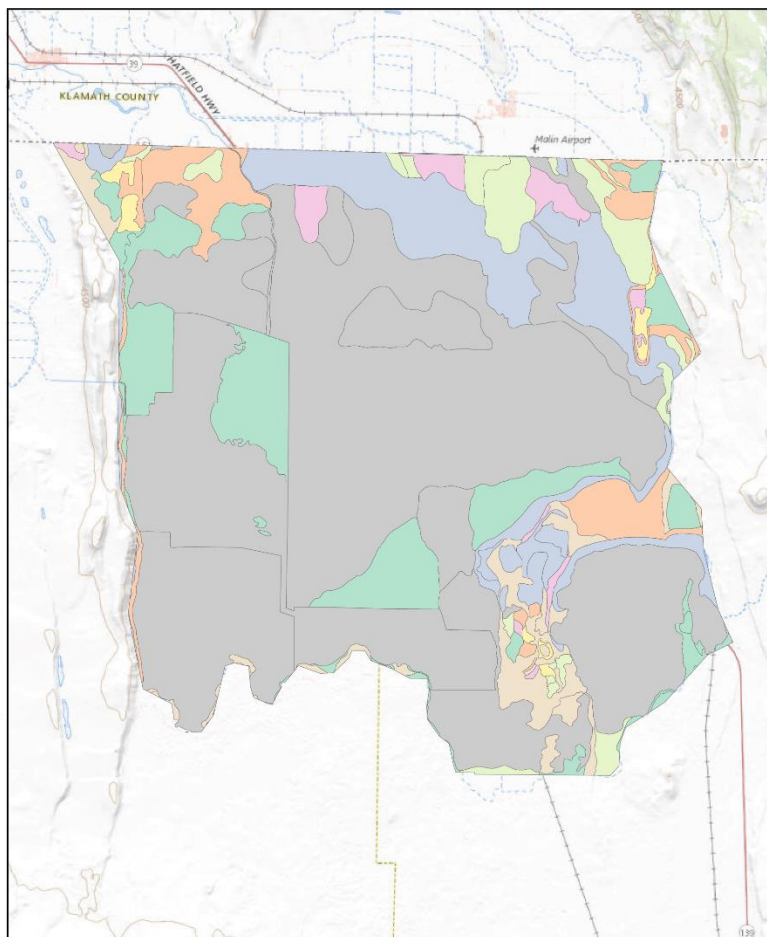


Figure 3: Soil map of the Tulelake Irrigation District [modified from the STATSGO2/SSURGO USDA NCRS database].

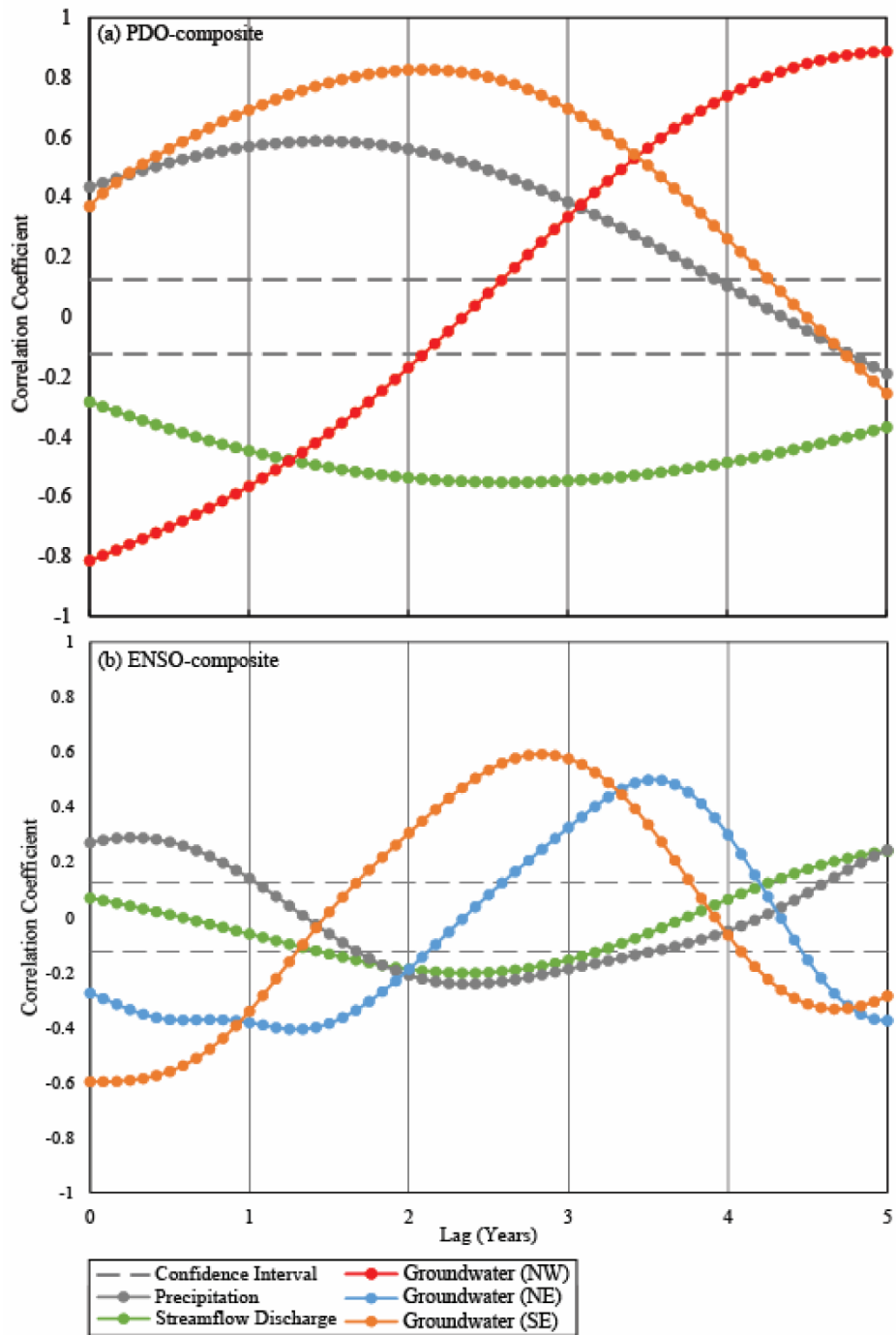


Figure 4: (a) Lag correlation of the PDO to hydrologic time series datasets (precipitation, streamflow discharge, and groundwater levels). (b) Lag correlation results of MEI to hydrologic time series datasets. The dashed grey lines on the plots correspond to a 95% confidence interval, and correlations above the confidence interval are statistically significant.

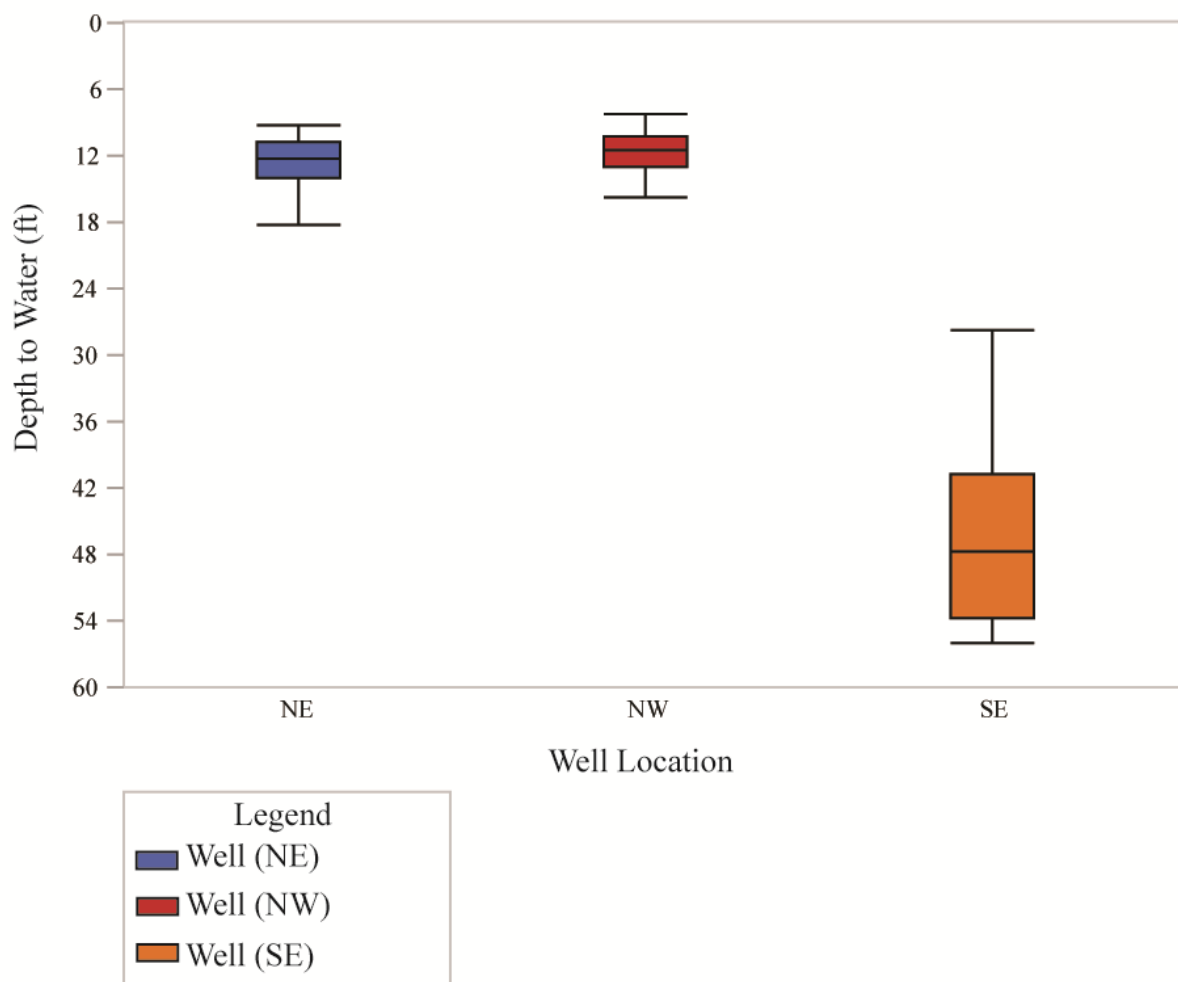


Figure 5: Box plots of depth to water measurement for three wells distributed in the northeast (NE), northwest (NW), and southeast (SE) quadrants in the Tulelake Irrigation District.

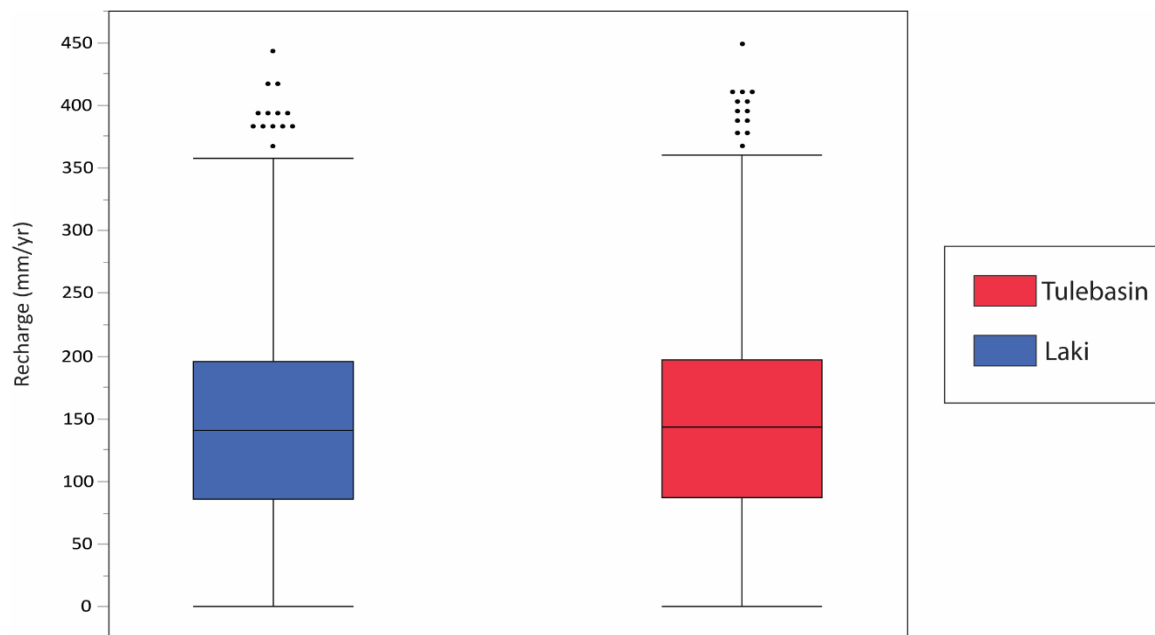


Figure 6: Cumulative annual recharge from 1950-2009 for the two common soil textures in the TID, Laki (blue) and Tulebasin soils (red).

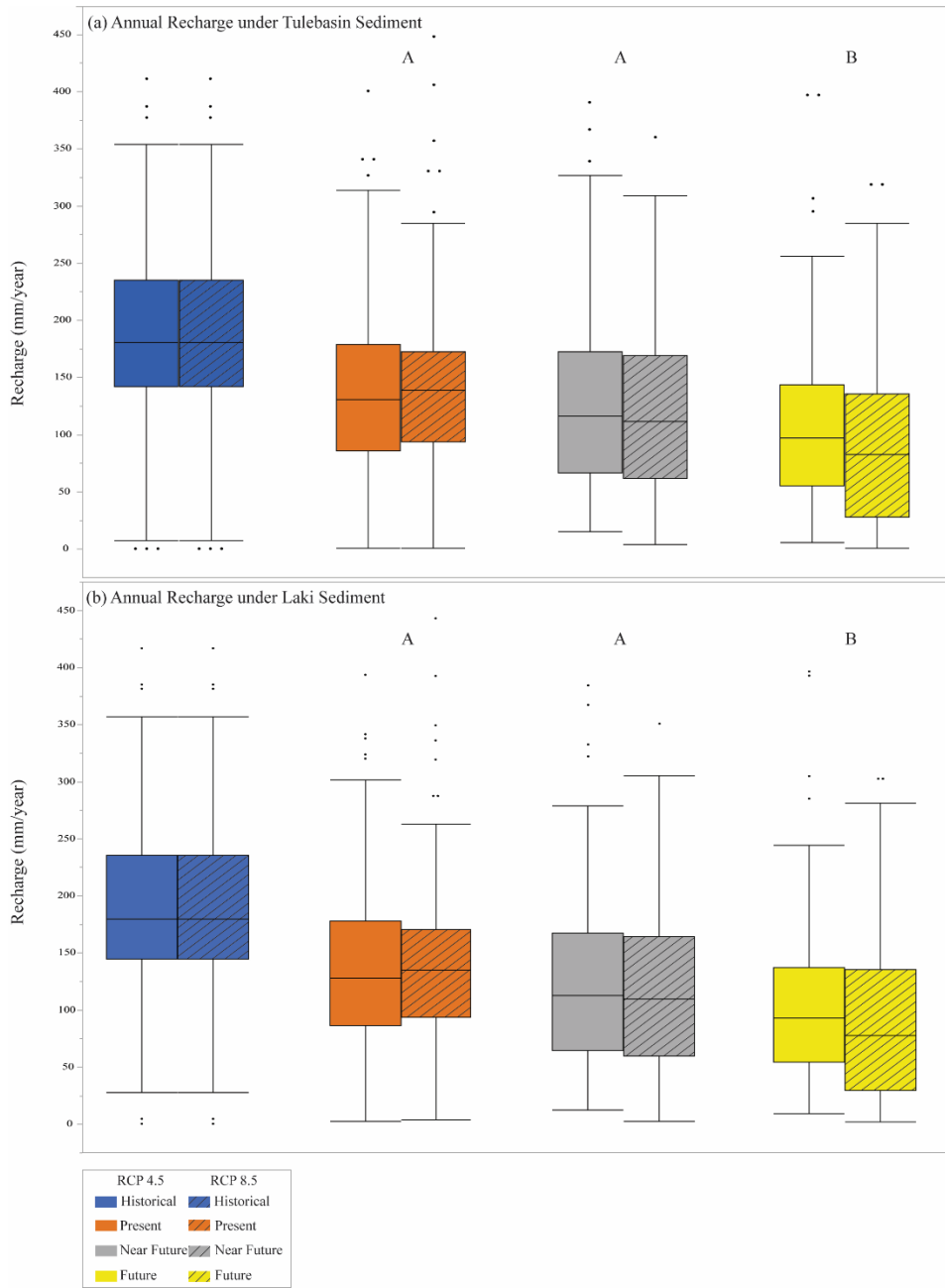


Figure 7: Cumulative annual recharge for the (a) Tulebasin sediment and (b) Laki sediment by time period for the representative concentration pathway (RCPs) 4.5 (solid) and 8.5 (hashed). Results from the Steel-Dwass test are shown above with letters denoting statistical differences from the historic time period.

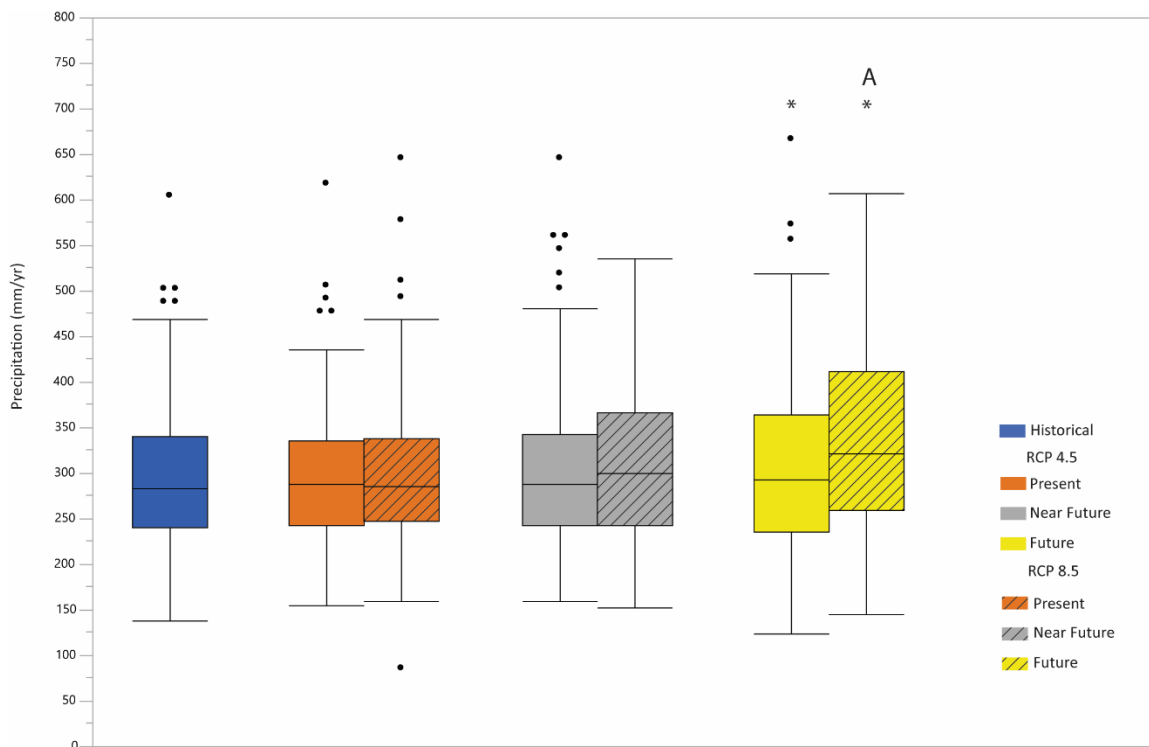


Figure 8: Cumulative annual precipitation by time period with historic and future projections from representative concentration pathways (RCPs) 4.5 and 8.5 of the global climate model (GCMs) datasets. Time periods correspond to: historical (1950-2005), present (2006-2039), near future (2049-2069), and future (2070-2099). Results from the Steel-Dwass test are shown above with letters denoting statistical differences from the historic time period, and asterisks denoting differences between 4.5 and corresponding 8.5 RCP datasets.

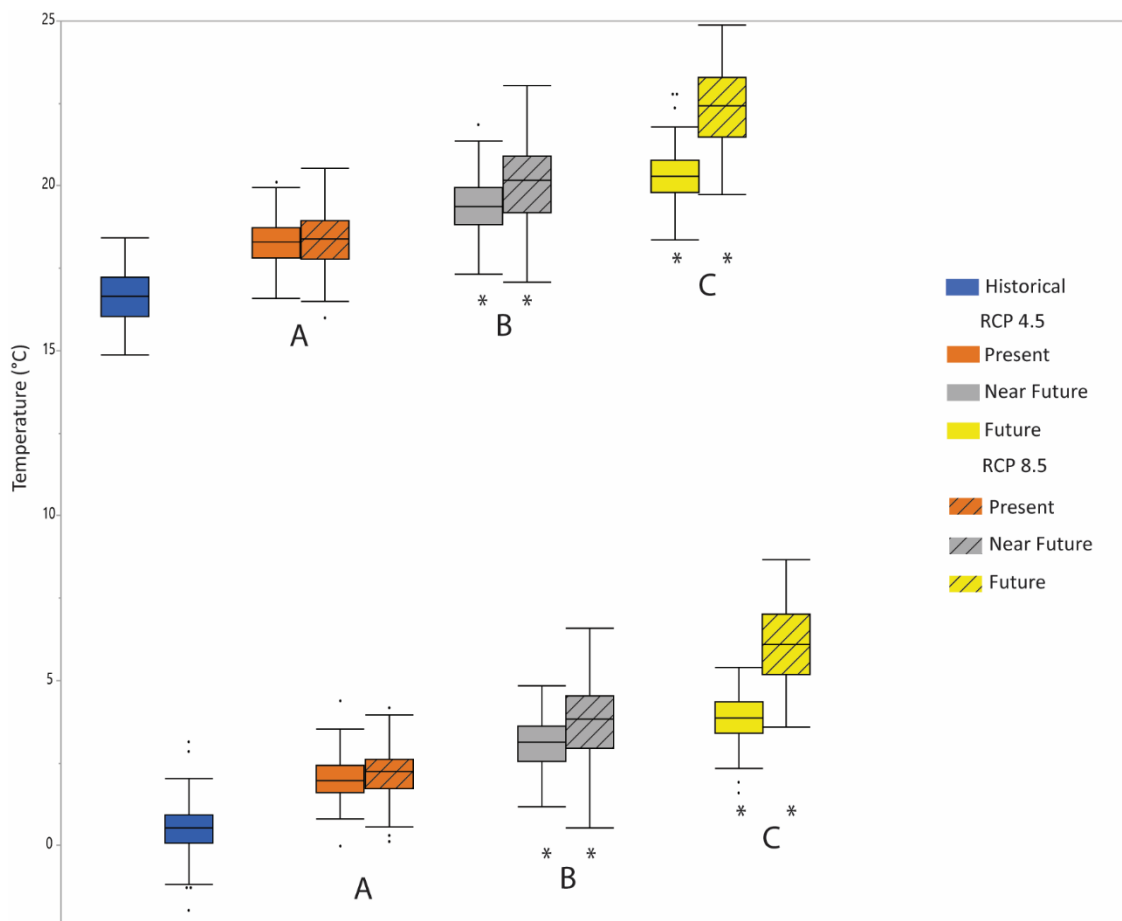


Figure 9: Temperature by time period with historic and future projections from representative concentration pathways (RCPs) 4.5 and 8.5 of the global climate model (GCMs) datasets. Time periods correspond to: historical (1950-2005), present (2006-2039), near future (2049-2069), and future (2070-2099). Lower values correspond to minimum temperature, and higher values correspond to maximum temperature. Results from the Steel-Dwass test are shown with letters denoting statistical differences from the historic time period, and asterisks denoting differences between 4.5 and corresponding 8.5 RCP datasets.

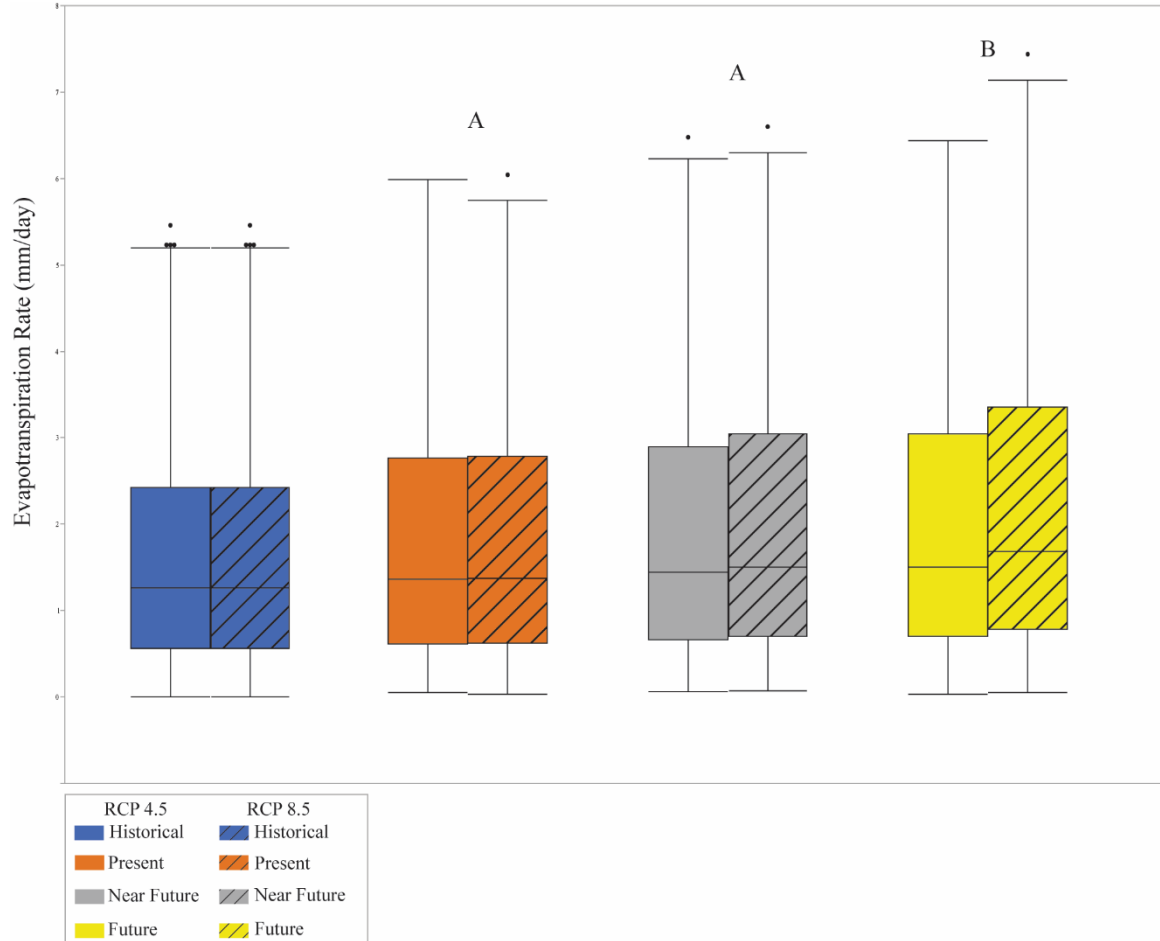


Figure 10: Evapotranspiration rate by time period for the cereal grains crop type with historic and future projections from representative concentration pathways (RCPs) 4.5 and 8.5 of the global climate model (GCMs) datasets. Results from the Steel-Dwass test are shown with letters denoting statistical differences from the historic time period.

7.0 Tables

Table 1: Summary of time series data used in the SSA and lag correlation analysis. Groundwater time series data summarized here was obtained from the CASGEM public repository. Precipitation time series data was obtained from the Climate Data Online (CDO) public repository, and streamflow discharge was obtained from the USGS NWIS public repository.

ID	Agency	Average Depth to Water (ft)	Starting Year	Ending Year	Record Length (Years)
Groundwater (NW)	CASGEM	11.9	2001	2019	18
Groundwater (NE)	CASGEM	10.2	2001	2019	18
Groundwater (SE)	USGS	46.9	2000	2019	19
Precipitation	NOAA CDO	--	1932	2018	86
Air Temperature (Tulelake)	NOAA CDO		1932	2018	86
Air Temperature (Lava Beds NM)	NOAA CDO		1959	2018	59
Streamflow Discharge	USGS NWIS	--	1921	2018	97

Table 2: Soil properties of native soils used as input for HYDRUS-1D models. θ_r , residual volumetric water content; θ_s , saturated volumetric water content; α and n , soil water retention function parameters; K_s , saturated hydraulic conductivity; and l , tortuosity parameter in the conductivity function.

Material	θ_r ($m^3 m^{-3}$)	θ_s ($m^3 m^{-3}$)	α ($m m^{-1}$)	n	K_s ($cm day^{-1}$)	l
Tulebasin	0.095	0.48	0.017	1.28	14.97	1
Laki	0.065	0.42	0.006	1.59	16.06	1

Table 3: The percent variance of the composite reconstructed components (RCs) attributed to the El Niño-Southern Oscillation (ENSO), Pacific Decadal Oscillation (PDO), and >PDO for the precipitation, streamflow, and groundwater-level timeseries. In the >PDO column, the period length (years) of the RC is denoted in the parentheses. The "--" denotes that no statistically significant RCs were detected.

	Percent Variance (%) of the Composite RCs		
Dataset	ENSO	PDO	>PDO
Precipitation	8.3%	37%	42% (43.5 years)
Streamflow	0.3%	6.0%	93% (99.1 years)
Groundwater (NW)	--	94%	--
Groundwater (NE)	26%	61%	--
Groundwater (SE)	15%	84%	--

Table 4: Results of the climate index to hydrologic time series lag correlations. Correlations are denoted between the Pacific Decadal Oscillation (PDO) and the El Niño-Southern Oscillation (ENSO) composite reconstructed components (RCs) of climate indices and precipitation, streamflow discharge, and groundwater levels. Minimum, maximum, and average correlation coefficients are denoted below with the corresponding lag time in years. The values in the grey boxes are not statistically significant based on the 95% confidence intervals shown in figure 4.

Index to Time Series	Minimum Correlation	Lag Time (years)	Maximum Correlation	Lag Time (years)	Average Correlation	Lag Time (years)
PDO – Precipitation	-0.22	5	0.59	1.3	0.35	3.1
PDO – Streamflow Discharge	-0.55	2.7	-0.28	0	-0.47	1.3
PDO – Groundwater (NW)	-0.81	0	0.89	5	0.07	2.5
PDO – Groundwater (NE)	-	-	-	-	-	-
PDO – Groundwater (SE)	-0.26	5	0.83	2.1	0.51	3.5
MEI – Precipitation	-0.24	2.3	0.29	0.25	-0.007	1.3
MEI – Streamflow Discharge	-0.20	2.3	0.24	5	-0.039	3.6
MEI – Groundwater (NW)	-	-	-	-	-	-
MEI – Groundwater (NE)	-0.41	1.33	0.50	3.5	-0.066	2.2
MEI – Groundwater (SE)	-0.60	0.08	0.59	2.8	-0.003	1.4